ACS APPLIED MATERIALS & INTERFACES

Research Article

www.acsami.org

Synthesis of Redox Polymer Nanobeads and Nanocomposites for Glucose Biosensors

Jen-Yuan Wang,[†] Lin-Chi Chen,*[,‡] and Kuo-Chuan Ho*[,†,§]

[†]Institute of Polymer Science and Engineering, [‡]Department of Bio-Industrial Mechatronics Engineering, and [§]Department of Chemical Engineering, National Taiwan University, Taipei 10617, Taiwan

Supporting Information

ABSTRACT: Redox polymer nanobeads of branched polyethylenimine binding with ferrocene (BPEI-Fc) were synthesized using a simple chemical process. The functionality and morphology of the redox polymer nanobeads were investigated by Fourier transform infrared spectroscopy (FTIR) and transmission electron microscopy (TEM). This hydrophilic redox nanomaterial could be mixed with glucose oxidase (GOx) for drop-coating on a screen-printed carbon electrode (SPCE) for glucose sensing application. Electrochemical properties of the BPEI-Fc/GOx/SPCE prepared under different conditions were studied by cyclic voltammetry (CV). On the basis of these CV results, the synthetic condition of the BPEI-Fc/GOx/SPCE could be optimized. By incorporating conductive poly(3,4-ethylenedioxythiophene):poly(styrenesulfonate) (PEDOT:PSS), the performance of a redox polymer nanobead–based enzyme electrode could be further improved. The influence of PEDOT:PSS on the nanocomposite enzyme electrode was discussed from the aspects of the apparent electron diffusion coefficient (D_{app}) and the charge transfer resistance (R_{ct}). The glucose-sensing sensitivity of the BPEI-Fc/PEDOT:PSS/GOx/SPCE is calculated to be 66 μA mM^{-1} cm^{-2}, which is 2.5 times higher than that without PEDOT:PSS. The apparent Michaelis constant (K_M^{app}) of the BPEI-Fc/PEDOT:PSS/GOx/SPCE estimated by the Lineweaver–Burk plot is 2.4 mM, which is much lower than that of BPEI-Fc/GOx/SPCE (11.2 mM). This implies that the BPEI-Fc/PEDOT:PSS/GOx/SPCE can catalytically oxidize glucose in a more efficient way. The interference test was carried out by injection of glucose and three common interferences: ascorbic acid (AA), dopamine (DA), and uric acid (UA) at physiological levels. The interferences of DA (4.2%) and AA (7.8%) are acceptable and the current response to UA (1.6%) is negligible, compared to the current response to glucose.

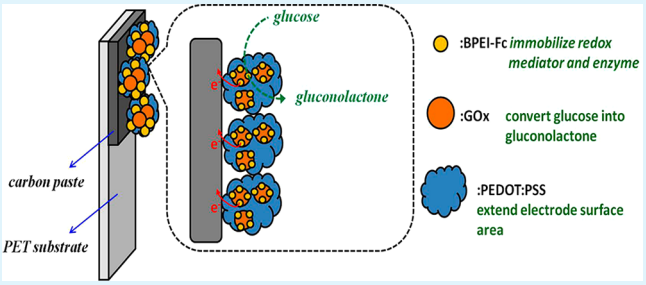

KEYWORDS: *ferrocene, glucose biosensor, glucose oxidase, PEDOT:PSS redox polymer, polyethyleneimine*

INTRODUCTION

Enzyme electrodes have been developed for several decades and widely used for bioelectronic devices, such as biosensors and biofuel cells, for their unique catalytic ability and selectivity.[1−4] According to the electron transfer mechanism, enzyme electrodes can be separated into two types,[5] namely, the direct one and indirect one. Direct electron transfer (DET) can be achieved using conducting nanomaterials, like carbon nanotubes[6] or graphene,[7] to directly "wire" the active site of the enzyme, thus accomplishing the electron transfer. To date, because of the thick protein shell around the active center of the enzyme, the biggest challenge has been to perform efficient DET between the electrode and the enzyme. The other type is mediator-based enzyme electrode, which utilizes a diffusible mediator, such as ferrocene (Fc)[8,9] or benzoquinone (BZQ),[10,11] to act as the electron shuttle. However, the leakage of these redox mediators remains as one of the main problems. To overcome the leakage problem in this system, immobilization of the redox mediators has been studied by many researchers in this field. Several nanostructured materials, such as functionalized carbon nanotubes and functionalized graphene, have exhibited the advantages on mediator immobilization, providing sufficient surface area for attachment and improving enzyme kinetics.[12−16] Wang et al.[12] reported an approach to form electrochemically functionalized multilayered nanostructures on the glassy carbon electrode through layer-by-layer (LBL) chemistry. Methylene green and positively charged functionalized multiwalled carbon nanotubes (MWCNTs) adsorbed on the electrode were used as examples of electroactive species. Qiu et al.[13] and Fan et al.[14] reported the direct linking of ferrocene with MWCNTs and graphene, and used as the glucose sensor and H_2O_2 sensor, respectively. Because the enzyme immobilization is accomplished through direct cross-linking on insulating chitosan, Pt nanoparticles and MWCNTs spacer are introduced to improve the sensitivity of the electrodes in the studies of Wu et al.[15] and Wan et al.[16]

Despite the conducting carbon nanomaterials, polymeric materials also show inspiring property in co-immobilization of

Received: May 15, 2013
Accepted: July 11, 2013
Published: July 11, 2013

redox mediators and enzymes. One approach is to entrap the mediators and enzymes during the electrochemical deposition of the polymer film. For example, the conducting polymer polypyrrole[17,18] was used in the pioneered work. The film thickness can be controlled by changing the accumulated charge during the electrochemical polymerization process. This method is attractive and the co-immobilization does not contain any chemical reaction. Thus, the activity of the enzyme can be well preserved. However, leaching of mediators and/or enzymes and diffusion resistance from the polymer matrices would potentially diminish the performances of the enzyme electrodes. An alternative approach is to employ a redox polymer gel as the three−dimensional matrices for enzyme immobilization. The redox polymer contains the pendants of redox species and the backbone polymer. Polymers such as poly(N-vinylimidazole) and poly(4-vinylpyridine) have been widely used for fixing redox mediators via chemical reaction.[19,20] There are several choices for the redox species, including osmium complex[21−23] and ferrocene[24,25] derivatives with cross-linkable functional groups. The redox potential of the polymeric material is tunable by changing the redox center or the tether length of the redox polymer. With this feature, various redox polymers have been designed and incorporated in different enzyme electrodes.[26]

One of the main factors in determining the performance of a polymer enzyme electrode for bioelectronic applications is the electron transfer efficiency. For example, slow electron hopping in a rigid, hydrophobic conducting polymer backbone would result in a low glucose-sensing current. Redox hydrogels, which consist of hydrophilic backbone and are covalently bounded with redox mediators, exhibit relatively high electron transfer efficiency.[27] This is because a soft, flexible, and hydrophilic redox hydrogel would not only be beneficial for electron hopping but also be good for ensuring homogeneous contacts between the enzyme and the mediator. Also, compared to the electropolymerization-entrapping method, the enzyme electrode prepared with a redox hydrogel is more simple and practical for real applications. Nevertheless, the insulating property of a hydrogel's polymer backbone would result in an electron-hopping barrier. One effective way to solve this problem is to incorporate some conducting materials, such as carbon nanotubes and Pt nanoparticles. Tran et al.[28] have incorporated single-walled carbon nanotubes into ferrocene-modified linear polyethylenimine (LPEI) redox polymer to increase the sensitivity for glucose sensing. MacAodha et al.[29] have used multiwalled carbon nanotubes and osmium redox polymer to obtain high and stable glucose oxidation current. Pan et al.[30] have reported a high-performance glucose biosensor with hierarchical nanostructured conducting polyaniline hydrogel. In Zhai et al. work,[31] the sensitivity is further improved by introducing Pt nanoparticle/polyaniline hydrogel heterostructures.

In this study, the redox polymer nanobeads, which preserve the original advantages of redox hydrogels but add another dimension of niches by considerably reducing the hydrogel size, are synthesized for glucose biosensors. The redox polymer nanobeads consist of branched polyethylenimine (BPEI) and Fc redox mediators. With good hydrophilicity, the BPEI-Fc nanobeads can form a well-dispersed aqueous solution. Under the neutral pH condition, glucose oxidase (GOx) is negatively charged and BPEI-Fc bears positive charges. Thus, GOx and BPEI-Fc can be blended well by electrostatic affinity. Besides, with lower chain flexibility the BPEI nanobeads can maintain their morphology and form nanocomposites with other materials. For instance, after further incorporation of conductive poly(3,4-ethylenedioxythiophene):poly-(styrenesulfonate) (PEDOT:PSS), we fabricate BPEI-Fc/PEDOT:PSS/GOx/SPCE that shows high glucose oxidation currents. Furthermore, the facile, simple and cost-effective process meets the need of the enzyme electrode fabrication from the practical aspects. In addition to the above synergistic role of BPEI-Fc and PEDOT:PSS, the morphologies of the BPEI−Fc nanobeads are observed by TEM analyses. The optimal synthetic condition of the redox polymer nanobeads is concluded from cyclic voltammetric (CV) analysis. The charge transfer resistances (R_{ct}) and the apparent electron diffusion coefficients (D_{app}) for the BPEI−Fc/GOx/SPCE and the BPEI-Fc/PEDOT:PSS/GOx/SPCE are characterized by electrochemical measurements (Tafel plots and Randles−Sevcik equation). Finally, the glucose-sensing sensitivity and selectivity of the enzyme electrodes are studied using an amperometric detection method.

EXPERIMENTAL SECTION

Chemicals. Branched polyethyleneimine (Sigma-Aldrich), ferrocenecarboxaldehyde (98%, Sigma-Aldrich), and sodium borohydride (95%, Riedel-de Haën) were used to synthesize the redox polymer nanobeads (BPEI-Fc). PEDOT:PSS (Clevios PH500) was used to form the redox nanocomposite with BPEI−Fc. For the enzyme electrode preparation, glucose oxidase (GOx, from *Aspergillusniger*, EC 1.1.3.4, 5000 U mL^{-1}, Sigma−Aldrich) and ethylene glycol diglycidyl ether (EDGDE, TCI America) were used as received. Monosodium phosphate monohydrate and disodium phosphate heptahydrate (ACS reagent, Sigma-Aldrich) were used to prepare the phosphate buffer solution with different pH values. Potassium chloride, D-(+)-glucose, and the interferences, ascorbic acid (AA) (>99%), uric acid (UA) (>99%), and dopamine hydrochloride (DA) were obtained from Sigma-Aldrich and used for the amperometric glucose sensing test.

Synthesis of Redox Polymer BPEI-Fc Nanobeads and BPEI-Fc/PEDOT:PSS Nanocomposite. The redox polymer nanobeads BPEI−Fc was prepared by coupling ferrocenecarboxaldehyde (FcCHO) to BPEI and following a similar protocol reported by Merchant et al.[32] First, 300 mg of BPEI was dissolved in 10 mL of anhydrous methanol. A solution of FcCHO was added drop wise into the well-dispersed BPEI solution, and the color of the mixture changed from pale yellow to dark orange. To study the effect of FcCHO amount, were tested six concentrations of FcCHO (0.5, 1.5, 2.0, 3.0, 4.0, and 5.0 mM). The mixture was stirred at 300 rpm for 3 h to complete the coupling reaction. The Schiff bases product could be stabilized by $NaBH_4$. After adding $NaBH_4$ (50 mg), the color of the resulting solution changed from dark red to pale yellow. Methanol was removed from the resulted mixture under reduced pressure, and the product was extracted with diethyl ether for 12 h to remove non−reacted FcCHO. The redox polymer was redissolved in methanol and filtered with the dialysis membrane (molecular weight cut-off, MWCO = 3500), and the methanol was removed under reduced pressure. BPEI−Fc/PEDOT:PSS was prepared by blending 2 mL of BPEI-Fc aqueous solution with 200 μL of PEDOT:PSS solution. This condition was to ensure a solution without aggregation after 1 h sonication. The resulted redox polymers and composites were stored at room temperature before use. The cross−linking between FcCHO and BPEI was verified by FTIR and electrochemical analyses. The particle size and zeta potential of the polymer were studied by DLS−Zetasizer.

Preparation of the BPEI-Fc/GOx/SPCE and the BPEI-Fc/PEDOT:PSS/GOx/SPCE. The enzyme electrodes were constructed as follows: 100 μL of redox polymer were first mixed with 100 μL of glucose oxidase (GOx, from *Aspergillusniger*, EC 1.1.3.4, 5000 U·mL^{-1}), and then 2 μL of the BPEI-Fc/GOx solution and 1 μL of EDGDE were drop-coated sequentially on a homemade screen-printed carbon electrode (SPCE) with an electrode area of 0.283 cm^2. Moreover, to achieve a uniform BPEI-Fc/GOx film, we treated the

SPCE with oxygen plasma (Plasma system FEMTO, Diener electronic, Germany) for 3 min before drop coating. After drop coating, the electrodes were placed in a laminar hood at 4 °C for 18 h to complete the cross-linking reaction. The electrodes were thoroughly dipped in 10 mL PBS (pH 7) to remove the non-cross-linked species. The constructed electrodes were stored in PBS (pH 7) at 4 °C before use, and they are denoted as BPEI-Fc/GOx/SPCE and BPEI-Fc/PEDOT:PSS/GOx/SPCE in this study, respectively.

Characterization. The functional group of BPEI-Fc was verified by FT−IR spectrometer (PerkinElmer Spectrum 100, USA). The morphology of BPEI-Fc was observed using transmission electron microscopy (TEM, JEOL JEM−1230, Japan). The standard three−electrode system was used to characterize the enzyme electrodes. The reference and counter electrodes were an Ag/AgCl/sat'd KCl electrode and a platinum sheet, respectively. The electrochemical measurements were carried out by an electrochemical workstation (CHI 900B, CHI, USA). Cyclic voltammetry (CV) was used to characterize the redox characteristics of the electrode, and obtain the cycling stability and eletrocatalytic activity for glucose oxidation. The cross-linking precursor's composition was also optimized based on the CV data. The kinetic parameters of the electrodes were obtained by performing Tafel analysis at a slow scan rate of 0.1 mV/s. The electrochemical impedance spectroscopy (EIS) measurements were carried out using a programmable potentiostat/galvanostat (Autolab PGSTAT30, Metrohm Autolab, Utrecht, The Netherlands). The glucose sensing experiments were performed according to our previous setup,[33] and the measuring potential was set at 0.45 V (vs. Ag/AgCl/sat'd KCl), which was determined from the linear sweep voltammograms (LSV) for catalytic glucose oxidation. The interference test was carried out by analyzing the amperometric *i*−*t* response of the BPEI−Fc/PEDOT:PSS/GOx/SPCE upon the injection of 3 mM glucose and three common interferences. The interferences selected for the test were 0.02 mM DA, 0.20 mM UA, and 0.05 mM AA. The concentrations of the interferences were set according to the average concentration in human body.

RESULTS AND DISCUSSION

Characterization of the BPEI-Fc/GOx/SPCE. Figure 1 shows the FTIR spectra of pristine BPEI and BPEI−Fc. For

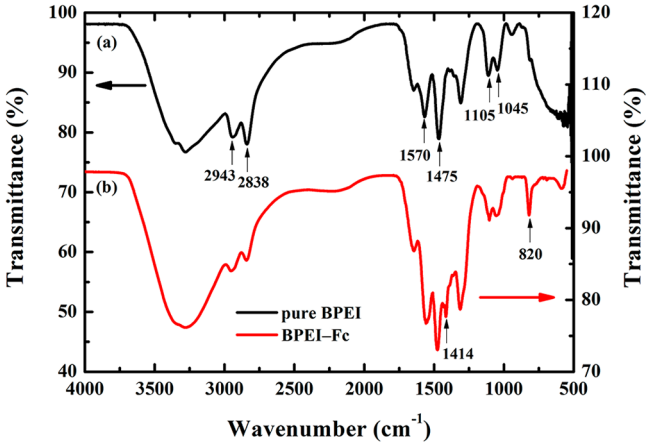

Figure 1. FTIR spectra of the (a) pure BPEI and (b) BPEI-Fc.

both polymers, the bending vibration of the NH_2 groups can be observed at 1560 cm^{-1}. The peaks at 1045 and 1105 cm^{-1} correspond to the symmetric and asymmetric stretching bands of imine groups, respectively. The absorption peaks at 1475, 2838, and 2943 cm^{-1} are ascribed to the symmetric and asymmetric stretching bands of CH_2, respectively. After binding FcCHO to the NH_2 group of BPEI, the characteristic peaks of ferrocene can be observed at 820 and 1414 cm^{-1}. From the results of DLS, the particle size of BPEI is changed after Fc coupling. Due to the abundant amino groups in the chemical structure, BPEI disperses uniformly in aqueous solution and the particle size is 7.1 nm. When the amino group is reacted with the aldehyde group of FcCHO, the hydrophobic structure would reduce the dispersion uniformity, thus the larger aggregation would appear. The DLS results of different BPEI−Fc are consistent with this observation and the particle sizes range between 100 and 400 nm. Figure 2a shows the TEM images of pure BPEI and BPEI−Fc. The shape of BPEI particle is irregular and the size ranges from 50 to 150 nm. After coupling with FcCHO, the amino groups on the BPEI were replaced by hydrophobic ferrocene. When there were more hydrophobic cores formed around the BPEI-Fc, the self-assembly of the BPEI−Fc nanobeads occurred, as the formation mechanism shown in Figure 2b. It is inferred that the amount of the hydrophobic part on the BPEI-Fc would affect the particle size directly. From the TEM images, the particle size of the BPEI-Fc is between 250 and 500 nm. The particle sizes obtained from the TEM are much larger than those obtained from the DLS. Since there is some aggregation of BPEI-Fc, the TEM data are consistent with the results of the DLS analysis. The size and zeta potential of redox polymer nanobead BPEI−Fc with different synthetic conditions are listed in Table 1. When the amount of FcCHO is increased during the synthesis, more BPEI-Fc coupling is achieved and the number of amino groups on the polymer chain is decreased. Thus, the decrease in the hydrophilicity of BPEI-Fc impairs the dispersion, and larger aggregates are formed. The size of BPEI−Fc increases gradually from 30.2 ([FcCHO] = 0.5 mM) to 555.9 nm ([FcCHO] = 5.0 mM). From the trend of the zeta potential of BPEI−Fc, a consistent result can be observed. The decrease of zeta potential implies that the stability of BPEI-Fc in solution is reduced, leading to more aggregation among each other.

To estimate the amount of redox mediator (Fc) anchored on the BPEI-Fc/GOx/SPCE and the BPEI−Fc/PEDOT:PSS/GOx/SPCE, the cyclic voltammograms (CVs) of the enzyme electrodes prepared with different concentrations of FcCHO were studied. Figure 3a shows the typical CVs of a BPEI-Fc enzyme electrode scanned between 0 and 0.75 V in a pH 5.5 PBS solution. The redox characteristics are contributed by ferrocene and the formal potential ($E^{0\prime}$) of Fc in the redox polymer system is 0.41 V. From the ratio of the oxidation and reduction peak current density (i_{pa}/i_{pc} = 0.97 at 50th cycle), the BPEI−Fc enzyme electrode shows good electrochemical reversibility. Owing to the hydrophilic property of BPEI, there is a 40% decrease in peak current after 50-cycle operation in the PBS solution, after which a stable peak current can be observed. While scanning the BPEI-Fc/GOx/SPCE prepared without using a cross-linking reagent, more severe desorption of BPEI-Fc from the electrode would take place (see the Supporting Information). Therefore, the cross-linking reagent plays a crucial role for binding the enzyme and the redox polymer nanobeads together on the enzyme electrode. Compared to glutaraldehyde, EDGDE is a better choice in this study (see the Supporting Infromation). By the following electrochemical relationship,[34] the surface coverage of BPEI-Fc on the enzyme electrode can be determined:

$$Q = nFA\Gamma \quad (1)$$

where Q represents the charge of the electrode, n is the electron transfer number, F is the Faraday's constant, A is the electrode surface area, and Γ is the surface coverage of BPEI-Fc.

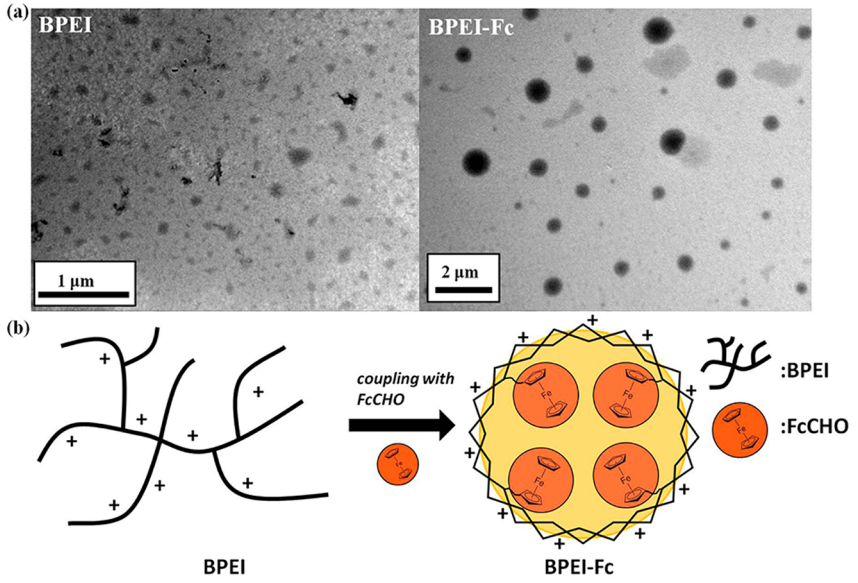

Figure 2. (a) TEM images of pure BPEI and BPEI-Fc. (b) The formation mechanism of the BPEI-Fc.

Table 1. Summary of the Characteristics of BPEI-Fc Redox Polymer Nanobeads with Different FcCHO Concentrations during Fabrication

sample	BPEI (mg)	FcCHO (mM)	surface coverage of Fc (mole cm^{-2})	size (from DLS) (nm)	zeta-potential (mV)
A	300	0.5	3.25×10^{-10}	30.2	3.79
B	300	1.5	7.93×10^{-10}	141.4	1.84
C	300	2.0	9.29×10^{-10}	180.5	1.68
D	300	3.0	1.16×10^{-9}	237.3	1.57
E	300	4.0	1.61×10^{-9}	367.4	1.35
F	300	5.0	1.79×10^{-9}	555.9	1.13

The surface coverage amounts of BPEI−Fc under different synthetic conditions are also listed in Table 1. Ranging from 3.25×10^{-10} to 1.79×10^{-9} mole cm^{-2}, the surface coverage of Fc on the enzyme electrode increases with the FcCHO concentration used in the BPEI-Fc coupling reaction. When the FcCHO concentration reaches 4.0 mM, there is no obvious increase of Γ, which infers that the saturation is achieved. Thus, the standard BPEI-Fc redox polymer nanobeads were prepared with 4.0 mM FcCHO, which resulted in an Fc surface coverage of 1.61×10^{-9} mole cm^{-2} on the enzyme electrode. Panels b and c in Figure 3 show the corresponding CVs and calibration curves of the BPEI-Fc enzyme electrode with different scan rates. The peak current shows linear dependence on the square root of the scan rate and obeys the Randles−Sevcik equation.[35]

$$i_p = \frac{0.4463 n^{3/2} F^{3/2} A D_{app}{}^{1/2} C \upsilon^{1/2}}{(RT)^{1/2}} \quad (2)$$

In eq 2, n is the electron transfer number, F is Faraday's constant, R is the gas constant (8.314 J mol^{-1} K^{-1}), T is the room temperature (298.15 K in our case), A is the area of the SPCE, D_{app} is the apparent electron diffusion coefficient, C is the effective electroactive site concentration, and υ is the scan rate. By plotting i_p *vs* $\upsilon^{1/2}$, the $D_{app}{}^{1/2}$ C can be estimated. C in the film can be calculated from the surface coverage Γ and the film thickness δ. The polymer loadings on all electrodes were fixed at 22.5 μg/electrode, and this condition yields a 1.2 μm−thick polymer film. For the BPEI-Fc enzyme electrode, C is 1.79×10^{-5} mole cm^{-3} and D_{app} is 5.4×10^{-11} cm^2 s^{-1}.

Characterization of the BPEI-Fc/PEDOT:PSS/GOx/SPCE. Figure 4 is the schematic of the BPEI-Fc/PEDOT:PSS/GOx/SPCE. Negatively charged PEDOT:PSS (zeta potential is −55.2 mV) can serve as the conductive surface for the positively charged BPEI-Fc nanoparticles. After blending BPEI-Fc with PEDOT:PSS, the zeta potential of the nanocomposite is 13.3 mV, this infers that the surface of the nanocomposite is covered with BPEI-Fc. Because GOx bears negative charge, the BPEI−Fc modified nanocomposite can also provide good immobilization substrate for preparing enzyme electrodes. Figure 5a shows the CVs of the BPEI-Fc/GOx/SPCE and the BPEI-Fc/PEDOT:PSS/GOx/SPCE. The latter electrode gives a higher redox current density and the surface coverage of the BPEI-Fc/PEDOT:PSS is calculated to be 4.24×10^{-9} mole cm^{-2}, which is 2.6 times higher than that of BPEI-Fc. The result indicates that a higher loading of BPEI-Fc can be achieved by using PEDOT:PSS. Although there is a slightly increase in $E^{0\prime}$, the electrode coated with BPEI-Fc/PEDOT:PSS shows good reversibility and stability. From the cycling stability analysis in Figure 5b, BPEI-Fc/PEDOT:PSS/GOx/SPCE shows better stability compared to that of BPEI−Fc. After 50 cycles, the oxidation peak current of the BPEI−Fc/PEDOT:PSS/GOx/SPCE remains 74% of its original one. From the CVs performed at different scan rates (Figure 5c), the value of D_{app} for the BPEI-Fc on the BPEI-Fc/PEDOT:PSS/GOx/SPCE is calculated to be 2.8×10^{-10} cm^2 s^{-1}, which is higher than that of BPEI-Fc/GOx/SPCE. These results imply that the BPEI-Fc/PEDOT:PSS/GOx/SPCE not only contains higher redox Fc capacity, but also exhibits a faster electron-hopping rate in the polymer film.

Another way to investigate the BPEI-Fc/PEDOT:PSS/GOx/SPCE and study the role of PEDOT:PSS is to use Tafel analysis. Tafel plot is a useful device for evaluating the kinetic parameters of the electrochemical systems.[36,37] Figure 6a shows the Tafel plots of the BPEI-Fc/GOx/SPCE and the BPEI-Fc/PEDOT:PSS/GOx/SPCE. The Tafel equation can be expressed by eq 3[38]

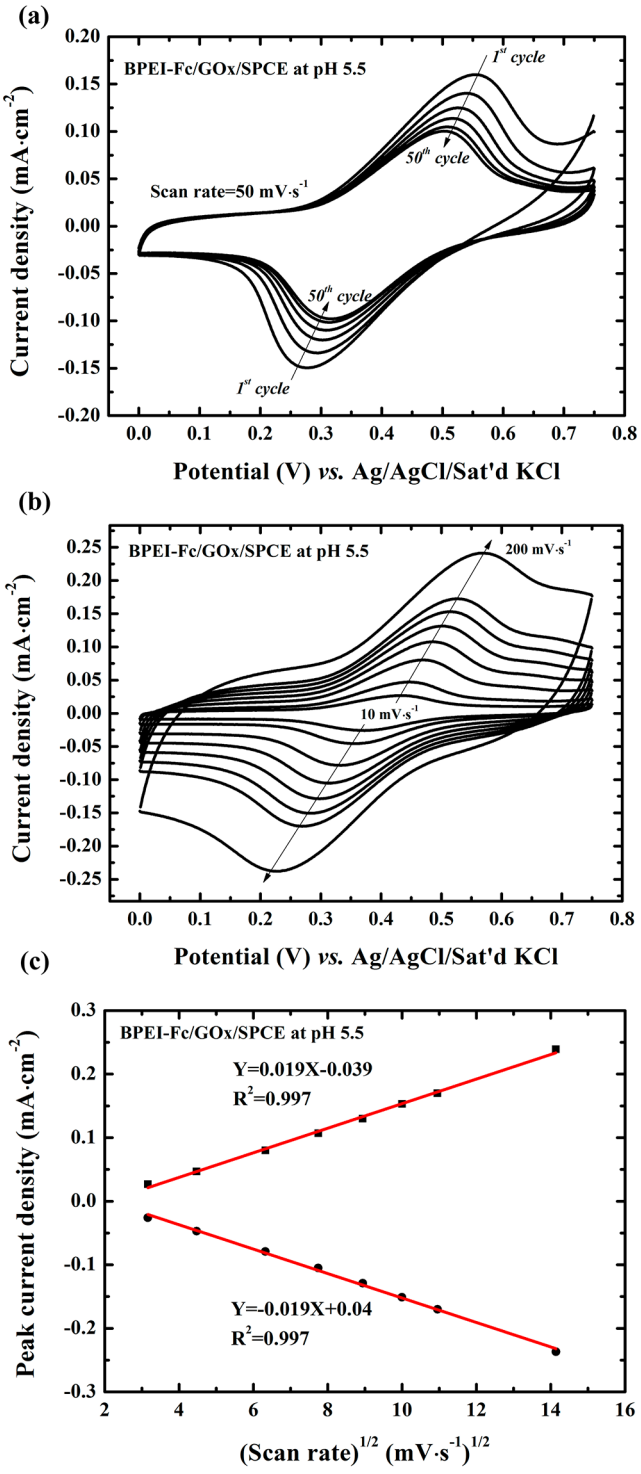

Figure 3. (a) CVs of the BPEI-Fc/GOx/SPCE for 50 cycles in PBS solution, pH 5.5 at a scan rate of 0.05 V/s. (The data shown every 10 cycle.) (b) The CVs of the BPEI-Fc/GOx/SPCE in PBS solution, pH5.5 with different scan rates. (c) Relationship between the peak current density of the BPEI-Fc/GOx/SPCE and the square root of the scan rate.

$$\log i = \log i_0 - \frac{\alpha n F(E - E^{0'})}{2.3RT} \quad (3)$$

where i represents the current, i_0 is the exchange current, α is the electron transfer coefficient, n is the electron transfer number, E is the applied voltage (V), $E^{0\prime}$ is the formal potential

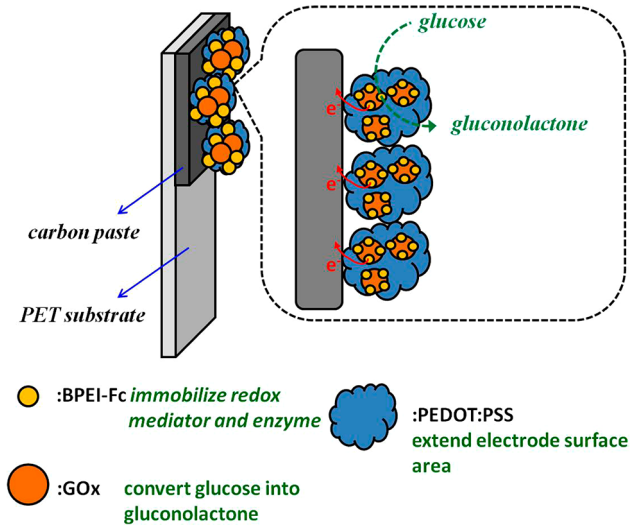

Figure 4. Schematic diagram of the BPEI-Fc/PEDOT:PSS/GOx/SPCE.

(V), F is Faraday's constant, R is the gas constant (8.314 J mol^{-1} K^{-1}), and T is the absolute temperature (298.15 K in our case). The exchange current, which reflects the intrinsic rate of electron transfer of the electrode at the formal potential, can be estimated by Tafel plots. For the BPEI-Fc/GOx/SPCE, the exchange current density ($j_0 = i_0/A$, where A is the area of the SPCE) is found to be 1.9×10^{-7} A cm^{-2}. Higher exchange current density (2.1×10^{-7} A cm^{-2}) can be observed for the enzyme electrode incorporated with PEDOT:PSS. According to the relationship between R_{ct} and exchange current density,[39] as shown in eq 4, the value of R_{ct} decreased after introducing PEDOT:PSS into the enzyme electrode. This result is consistent with the EIS results obtained in Figure 6b. In the impedance spectra, the R_{ct} is improved from 1650 to 850 Ω after introducing PEDOT:PSS. Besides, there is an obvious shift (ca. 0.025 V) of the formal potential after combining PEDOT:PSS with BPEI−Fc. This slight potential shift infers that the BPEI−Fc/PEDOT:PSS/GOx/SPCE gives a relatively low overpotential. In this system, PEDOT:PSS provides a facile kinetic pathway and enhances the electron transfer rate in the polymer film.

$$R_{ct} = \frac{RT}{Fi_0} \quad (4)$$

Glucose Sensing of BPEI-Fc/GOx/SPCE and BPEI-Fc/PEDOT:PSS/GOx/SPCE. Figure 7a shows the influence of pH value on the electrochemical behavior of the BPEI−Fc/PEDOT:PSS/GOx/SPCE. When the pH value is changed from 5.5 to 8, $E^{0\prime}{}_{BPEI-Fc}$ shifts toward a negative direction (0.403 to 0.325 V). Besides, there is also a decrease of current density, and the BPEI−Fc encounters an incomplete oxidation of Fc in PBS at pH 8.0. The glucose electrocatalytic current densities on the BPEI−Fc/PEDOT:PSS/GOx/SPCE in PBS with different pH values containing 2.0 mM glucose are presented in Figure 7b. A decrease of electrocatalytic current density is noticed when the pH value is increased from 5.5 to 8.0. For both BPEI-Fc/GOx/SPCE and BPEI-Fc/PEDOT:PSS/GOx/SPCE, the highest electrocatalytic current density is found at pH 5.5. Therefore, the operating condition is set at pH 5.5, and this is also a suitable environment for GOx to keep its activity. Figure 8a shows the results of the

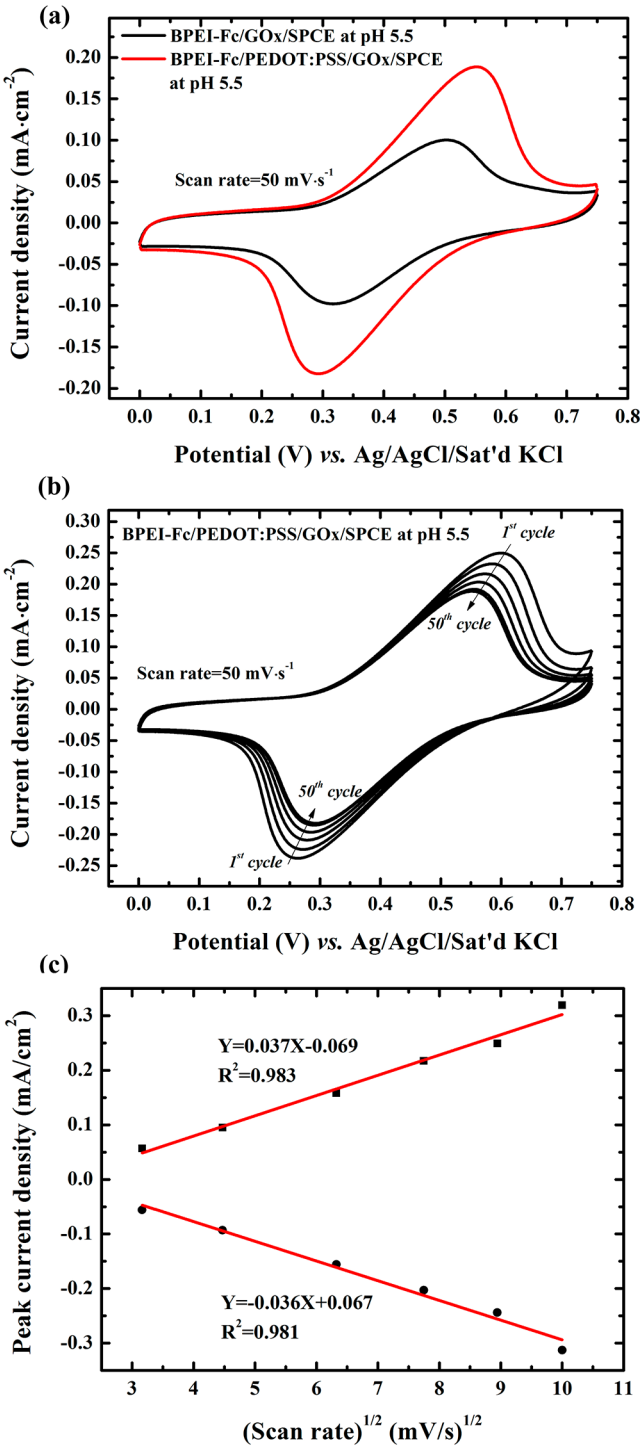

Figure 5. (a) CVs of the BPEI-Fc/GOx/SPCE and the BPEI-Fc/PEDOT:PSS/GOx/SPCE in PBS solution, pH 5.5 at a scan rate of 0.02 V/s. (b) CVs of the BPEI-Fc/PEDOT:PSS/GOx/SPCE for 50 cycles in PBS solution, pH 5.5 at a scan rate of 0.05 V/s (the data show every tenth cycle). (c) Relationship between the peak current density of BPEI-Fc/PEDOT:PSS/GOx/SPCE and the square root of the scan rate.

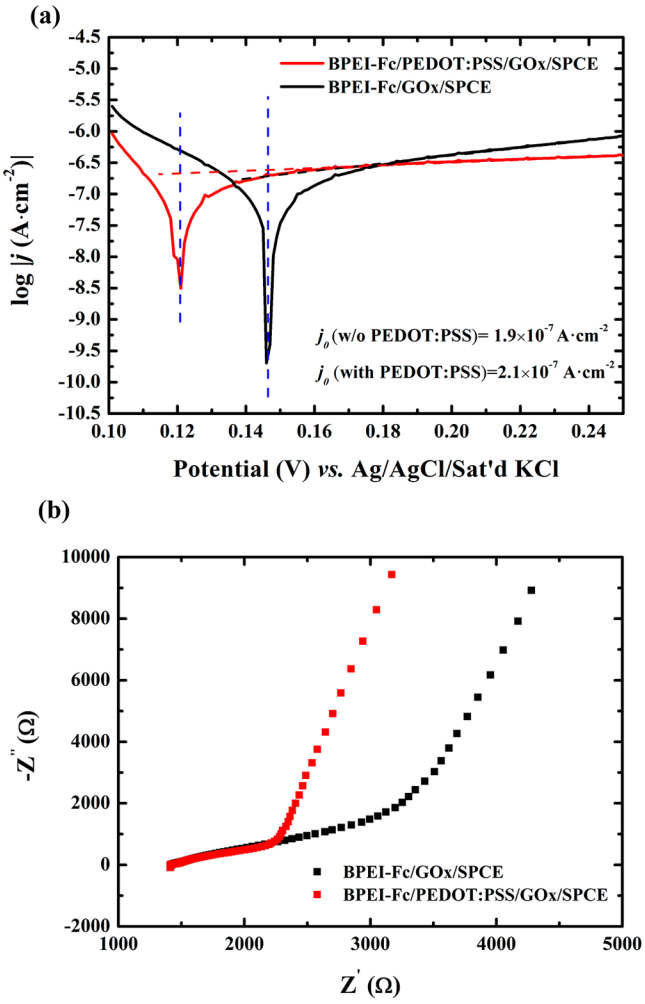

Figure 6. (a) Tafel plots of the BPEI-Fc/GOx/SPCE and the BPEI-Fc/PEDOT:PSS/GOx/SPCE in PBS solution at pH 5.5. (b) EIS of the BPEI-Fc/GOx/SPCE and the BPEI-Fc/PEDOT:PSS/GOx/SPCE.

amperometric response of glucose against the BPEI−Fc/GOx/SPCE and the BPEI−Fc/PEDOT:PSS/GOx/SPCE. Amperometric measurements of the electrodes were done at a constant applied potential of 0.45 V (vs. Ag/AgCl). In the range of 0.5−10 mM, the responses show obvious increases with each injection of 0.5 mM glucose for both BPEI-Fc/GOx/SPCE and BPEI-Fc/PEDOT:PSS/GOx/SPCE. The response time of glucose on the BPEI−Fc/GOx/SPCE reaches 95% of its steady-state value in about 32 s for each glucose injection. With the incorporation of PEDOT:PSS, the response time decreases to about 22 s, and the current response increases significantly. From the corresponding calibration curves of the enzyme electrodes shown in Figure 8b, both electrodes give linear behavior to glucose in 0.5 to 4.5 mM. The sensitivities of the BPEI-Fc/GOx/SPCE and the BPEI−Fc/PEDOT:PSS/GOx/SPCE are 27 and 66 μA mM^{-1} cm^{-2} (with the correlation coefficients of 0.988 and 0969), respectively. Table 2 is a mostly complete list of the glucose biosensors studied based on ferrocene-modified polymers and carbon materials. Because the substrate of BPEI-Fc enzyme electrode is screen-printed carbon, compared to more conductive glassy carbon electrode, a larger potential is required (0.45 V) and the BPEI-Fc/PEDOT:PSS/GOx/SPCE shows attractive performance comparing to the others.

Generally, the current responses of the enzyme electrodes can be described by the Michaelis−Menten kinetics.[40] The Lineweaver−Burk plot (shown in Figure 8c) can be written according to the following equation[41]

dx.doi.org/10.1021/am4018219 | ACS Appl. Mater. Interfaces 2013, 5, 7852−7861

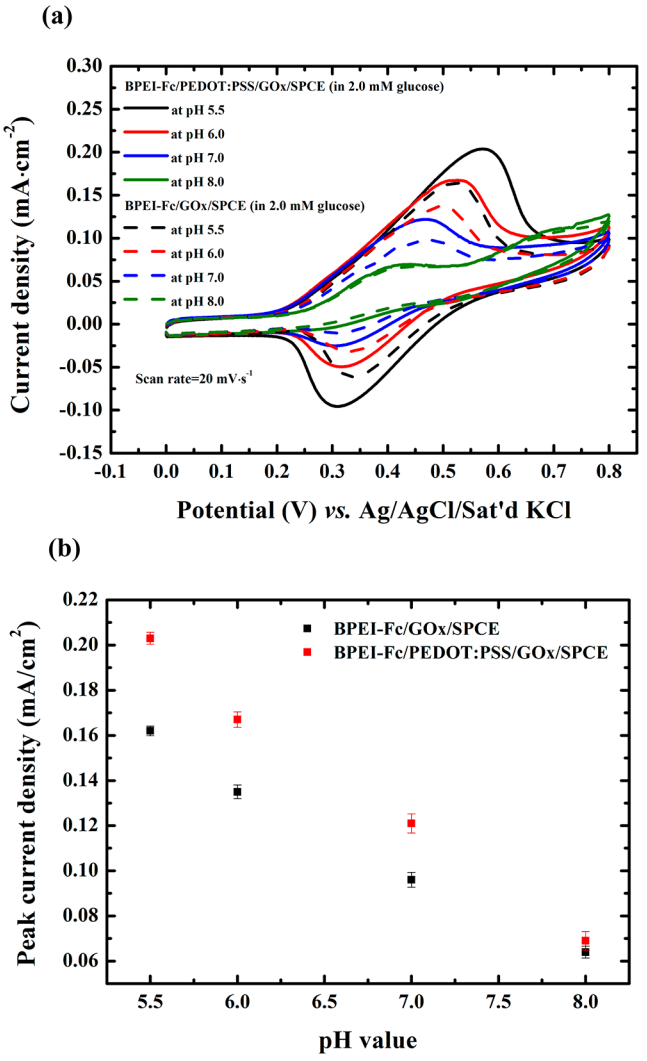

Figure 7. (a) CVs of the BPEI-Fc/GOx/SPCE and the BPEI-Fc/PEDOT:PSS/GOx/SPCE in PBS solutions with different pH values. (b) Peak current density of the BPEI-Fc/GOx/SPCE and the BPEI-Fc/PEDOT:PSS/GOx/SPCE in PBS solutions with different pH values.

$$\frac{1}{i_{ss}} = \frac{1}{i_{max}} + \frac{K_M^{app}}{i_{max}}\frac{1}{C_g} \quad (5)$$

where i_{ss}, i_{max}, C_g, and K_M^{app} are the steady-state current after adding glucose, the maximum response current, glucose concentration, and the apparent Michaelis constant of the electrode, respectively. The value of K_M^{app} for the BPEI–Fc/PEDOT:PSS/GOx/SPCE estimated from Figure 8c is 2.4 mM, which is much smaller than that of BPEI-Fc/GOx/SPCE (11.2 mM) and the native GOD in the same solution (27.0 mM).[42] This result implies that the GOx immobilized on the electrode with PEDOT:PSS shows stronger affinity to glucose. Another advantage in adding PEDOT:PSS can be observed is the parameter i_{max}, which is related to the efficiency of glucose oxidation for the electrodes. The higher i_{max} of the BPEI-Fc/PEDOT:PSS/GOx/SPCE (1.34 mA cm^{-2}) reveals the electrode with PEDTO:PSS has high activity for GOx. Table 3 summarizes the glucose biosensors including redox hydrogels and conductive polymer hydrogels. The BPEI-Fc/PEDOT:PSS/GOx/SPCE gives comparable performance to most of the previous studies.

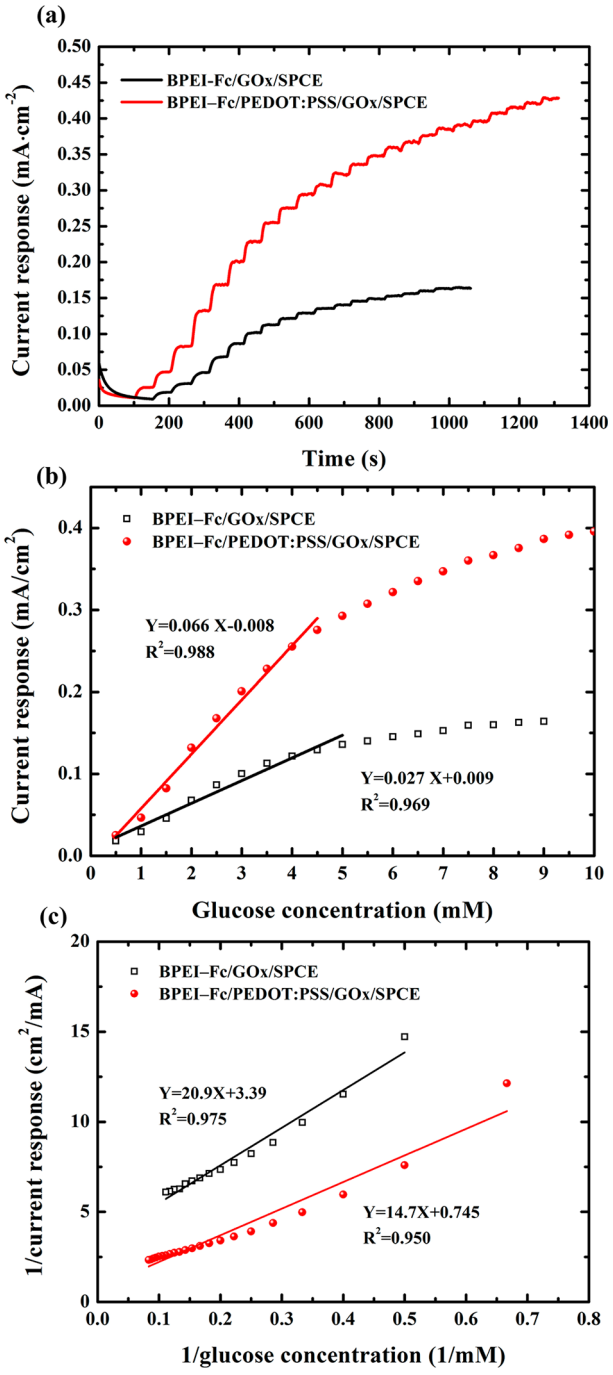

Figure 8. (a) Amperometric i–t response of the BPEI-Fc/GOx/SPCE and the BPEI-Fc/PEDOT: PSS/GOx/SPCE for the addition of different glucose concentrations in PBS solution, pH 5.5. (b) Calibration curves of glucose electrocatalytic current response of the BPEI-Fc/GOx/SPCE and the BPEI-Fc/PEDOT:PSS/GOx/SPCE. (c) Lineweaver–Burk plot of the BPEI-Fc/GOx/SPCE and the BPEI-Fc/PEDOT:PSS/GOx/SPCE.

Interference Effect on the Response of the BPEI–Fc/PEDOT:PSS/GOx/SPCE. Figure 9 shows the amperometric response of the BPEI-Fc/PEDOT:PSS/GOx/SPCE upon the injection of 3.0 mM glucose and three common interferences. The interferences selected for the test were 0.02 mM dopamine (DA), 0.20 mM uric acid (UA), and 0.05 mM ascorbic acid (AA). The concentrations of the interferences were chosen based on their average concentration in human body.[30] The

dx.doi.org/10.1021/am4018219 | ACS Appl. Mater. Interfaces 2013, 5, 7852–7861

Table 2. Mostly Complete List of the Glucose Biosensors Based on Ferrocene-Modified Polymers and Carbon Materials

electrode	potential (V vs. Ag/AgCl)	linear range (mM)	sensitivity (μA cm^{-2} mM^{-1})	ref
GOD/MWNTs-Fc/CS/GCE	0.35	0.012−3.8	25	13
LPEI-Fc/GCE	0.4 (SCE)	0.005−0.1	73	32
$PyCO_2H$[a]/Ppy[b]-Fc/GOx/GCE	0.38	1.0−4.0	1.796	43
MWCNT-PAP[c]-Fc/ITO	0.35	5.0−50	0.83	44
FC-20[d]/Chi/GOx/GCE	0.45	1.0−6.0	0.86	45
GNPs/CD-Fc/GOD/GCE	0.25 (SCE)	0.08−11.5	18.2	46
FMC/AMWNTs[e]/GCE	0.35	0.01−4.2	10.56	47
Th[g]/$ThCO_2H$[h]/ThFc[i]	0.35	0.5−3.0	0.04	48
FMC-BSA[j] /MWNTs/ormosil/GCE	0.3	0.05−20	0.26	49
GOx/C_{60}-Fc-CS-IL/GCE[k]	0.1	10^{-5}−0.01	234.67	50
CS-Fc/MWCNTs/GCE	0.35	0.005−1.5	13.08	51
FMC/Nafion/GOx/SWCNT	0.8	0.25−3.0	9.32	52
BPEI-Fc/GOx/SPCE	0.45	0.5−4.5	27	this work
BPEI-Fc/PEDOT:PSS/GOx/SPCE	0.45	0.5−4.5	66	this work

[a]$PyCO_2H$: ferrocenemonocarboxylicacid-modified 3-(aminopropyl) triethoxysilane. [b]Ppy: polypyrrole. [c]PAP: poly-aminoethylphenylene. [d]FC-20: ferrocene-substituted polysiloxane. [e]FMC/AMWNTs: ferrocene monocarboxylic acid-modified 3-(aminopropyl) triethoxy-silane enwrapping multiwalled carbon nanotubes. [f]$FcMe_2$-C_3-LPEI: 3-(dimethylferrocenyl) propyl-modified LPEI. [g]Th: poly(thiophene). [h]$ThCO_2H$: poly(3-thiophene acetic acid). [i]ThFc: dicyclopentadienyl iron-1,4-dienylmethyl-2-(thiophen-3-yl)acetate. [j]FMC-BSA: ferrocene monocarboxylic acid-bovine serum albumin. [k]C_{60}-Fc-CS-IL-GCE: the conjugation of fullerene, ferrocene, chitosan, ionic liquid, and glucose oxidase (GOx).

Table 3. List of the Glucose Biosensors Based on Redox Hydrogels and Conductive Polymer Hdyrogels

electrode	potential (V vs. Ag/AgCl)	linear range (mM)	sensitivity (μA cm^{-2} mM^{-1})	ref
PEDOT/GOx/Pt	0.35	0.1−10	12.42	11
GOx−PAni[a] hydrogel/Pt	−0.3 (SCE)	0.1−2.6	85.4	30
GOx/PtNP/PAni/Pt	−0.56 (SCE)	0.01−8	96.1	31
PAAm[b]/PAA[c]/PEDOT/GOx/	0.3	1−12	10	53
Alg-Ppy[d]/R[e]/Pt	0.35	5.0−50	7.8	54
BPEI-Fc/GOx/SPCE	0.45	0.5−4.5	27	this work
BPEI-Fc/PEDOT:PSS/GOx/SPCE	0.45	0.5−4.5	66	this work

[a]PAni: polyaniline. [b]PAAm: polyacrylamide. [c]PAA: poly(bis-acrylamide). [d]Alg-Ppy: alginate polypyrrole. [e]R: the conjugation of biotinylated-glucose oxidase and biotinylated-polypyrrole through avidin bridges.

oxidation potentials of DA and AA are 0.3 and 0.2 V (vs. Ag/AgCl), respectively. In this study, the operating potential of the glucose sensor gives sufficient overpotential for DA and AA to be oxidized. Because the glucose sensing potential on the BPEI-Fc/PEDOT:PSS/GOx/SPCE was much higher than the oxidation potential of DA and AA, it was hard to avoid the electrochemical reactions from the interferences. During the amperometric measurement, the oxidation currents of DA and AA could be observed, which were 4.2 and 7.8% of the current in response to 3.0 mM glucose, respectively. These results imply that the positively charged BPEI−Fc/PEDOT:PSS on the enzyme electrode cannot act as an effective permselective membrane for DA and AA. However, the high current response of glucose made the interferences of DA and AA acceptable. Moreover; the current response against 0.20 mM of UA was negligible compared to the current response to 3.0 mM for glucose.

CONCLUSIONS

In this study, redox polymer beads BPEI-Fc was successfully synthesized and characterized by FTIR and electrochemical measurements. From the investigation of DLS and TEM analyses, the average particle sizes were 250 and 350 nm, respectively. Besides, the spherical BPEI-Fc was stable and well−dispersed in aqueous solution. After being coated on the homemade SPCE, BPEI-Fc also possessed good electrochemical reversibility. In order to further improve this redox polymer, PEDOT:PSS was introduced to form a redox nanocomposite. From the results of D_{app} and R_{ct} for the BPEI-Fc/PEDOT:PSS/GOx/SPCE, the diffusion and electron transfer rate could be enhanced by incorporating PEDOT:PSS. Moreover, the formal potential of the BPEI-Fc/PEDOT:PSS/GOx/SPCE decreased slightly and a relatively low driving potential was required to accomplish the oxidation of BPEI-Fc. Thus, the BPEI-Fc/PEDOT:PSS/GOx/SPCE shows remarkable improvement in sensitivity against glucose. This study demonstrates a simple and effective way to improve the BPEI-Fc/GOx/SPCE for glucose sensing.

ASSOCIATED CONTENT

Supporting Information

CVs of the BPEI-Fc/GOx/SPCE prepared without cross-linker and with glutaaldehyde (GA) cross-linker. This material is available free of charge via the Internet at http://pubs.acs.org.

AUTHOR INFORMATION

Corresponding Author

*E-mail: chenlinchi@ntu.edu.tw (L-C.C.); kcho@ntu.edu.tw (K-C.H.). Fax: +886-2-2362-7620 (L-C.C.); +886-2-2362-3040 (K-C.H.). Tel: +886-2-3366-5343 (L-C.C.); +886-2-2366-0739 (K-C.H.).

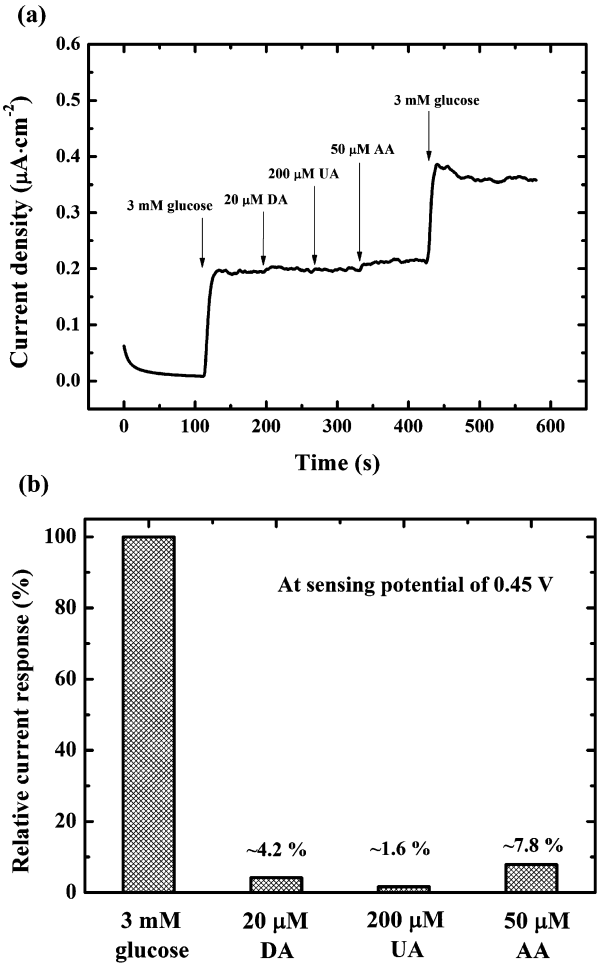

Figure 9. (a) Amperometric *i*–*t* response of the BPEI–Fc/PEDOT:PSS/GOx/SPCE to the injection of 3 mM glucose and three common interferences: 0.02 mM DA, 0.20 mM UA, and 0.05 mM AA. The working potential was 0.45 V. (b) Current response of to glucose (set as 100%), DA, UA, and AA of the BPEI-Fc/PEDOT:PSS/GOx/SPCE.

Notes

The authors declare no competing financial interest.

■ ACKNOWLEDGMENTS

This work was supported by the National Science Council of Taiwan under Grant 100-2628-E-002-032-MY2).

■ REFERENCES

(1) Sarma, A. K.; Vatsyayan, P.; Goswami, P.; Minteer, S. D. *Biosens. Bioelectron.* **2009**, *24*, 2313–2322.
(2) Willner, I.; Katz, E. *Angew. Chem., Int. Ed.* **2000**, *39*, 1180–1218.
(3) Bullen, R. A.; Arnot, T. C.; Lakeman, J. B.; Walsh, F. C. *Biosens. Bioelectron.* **2006**, *21*, 2015–2045.
(4) Davis, F.; Higson, S. P. J. *Biosens. Bioelectron.* **2007**, *22*, 1224–1235.
(5) Yu, E. H.; Scott, K. *Energies* **2010**, *3*, 23–42.
(6) Jose, M. V.; Marx, S.; Murata, H.; Koepsel, R. R.; Russell, A. J. *Carbon* **2012**, *50*, 4010–4020.
(7) Liu, X.; Shi, L.; Niu, W.; Li, H.; Xu, G. *Biosens. Bioelectron.* **2008**, *23*, 1887–1890.
(8) Qiu, J.-D.; Xiong, M.; Liang, R.-P.; Peng, H.-P.; Liu, F. *Biosens. Bioelectron.* **2009**, *24*, 2649–2653.
(9) Yang, W.; Zhou, H.; Sun, C. *Macromol. Rapid Commun.* **2007**, *28*, 265–270.
(10) Qingmei, Z.; Qingji, X.; Yingchun, F.; Zhaohong, S.; Xue'en, J.; Shouzhuo, Y. *J. Phys. Chem. B* **2007**, *111*, 11276–11284.
(11) Nien, P.-C.; Tung, T.-S.; Ho, K.-C. *Electroanalysis* **2006**, *18*, 1408–1415.
(12) Wang, X.; Wang, J.; Cheng, H.; Yu, P.; Ye, J.; Mao, L. *Langmuir* **2011**, *27*, 11180–11186.
(13) Qiu, J.-D.; Zhou, W.-M.; Guo, J.; Wang, R.; Liang, R.-P. *Anal. Biochem.* **2009**, *385*, 264–269.
(14) Fan, L.; Zhang, Q.; Wang, K.; Li, F.; Niu, L. *J. Mater. Chem.* **2012**, *22*, 6165–6170.
(15) Wu, H.; Wang, J.; Kang, X.; Wang, C.; Wang, D.; Liu, J.; Aksay, I. A.; Lin, Y. *Talanta* **2009**, *80*, 403–406.
(16) Wan, D.; Yuan, S.; Li, G. L.; Neoh, K. G.; Kang, E. T. *ACS Appl. Mater. Interfaces* **2010**, *2*, 3083–3091.
(17) Foulds, N. C.; Lowe, C. R. *J. Chem. Soc., Faraday Trans.* **1986**, *82*, 1259–1264.
(18) Umana, M.; Waller, J. *Anal. Chem.* **1986**, *58*, 2979–2983.
(19) Happ, B.; Winter, A.; Hager, M. D.; Schubert, U. S. *Chem. Soc. Rev.* **2012**, *41*, 2222–2255.
(20) Coman, V.; Gustavsson, T.; Finkelsteinas, A.; von Wachenfeldt, C.; Hagerhall, C.; Gorton, L. *J. Am. Chem. Soc.* **2009**, *131*, 16171–16176.
(21) Shin, H.; Cho, S.; Heller, A.; Kang, C. *J. Electrochem. Soc.* **2009**, *156*, F87–F92.
(22) Prevoteau, A.; Mano, N. *Electrochim. Acta* **2012**, *68*, 128–133.
(23) Heller, A. *Curr. Opin. Chem. Biol.* **2006**, *10*, 664–672.
(24) Sulak, M. T.; Gokdogan, O.; Gulce, A.; Gulce, H. *Biosens. Bioelectron.* **2006**, *21*, 1719–1726.
(25) Dai, Z. H.; Ni, J.; Huang, X. H.; Lu, G. F.; Bao, J. C. *Bioelectrochemistry* **2007**, *70*, 250–256.
(26) Sassolas, A.; Blum, L. J.; Leca-Bouvier, B. D. *Biotechnol. Adv.* **2012**, *30*, 489–511.
(27) Oldenziel, W. H.; Westerink, B. H. C. *Anal. Chem.* **2005**, *77*, 5520–5528.
(28) Tran, T. O.; Lammert, E. G.; Chen, J.; Merchant, S. A.; Brunski, D. B.; Keay, J. C.; Johnson, M. B.; Glatzhofer, D. T.; Schmidtke, D. W. *Langmuir* **2011**, *27*, 6201–6210.
(29) MacAodha, D.; Luisa Ferrer, M.; Conghaile, P. O.; Kavanagh, P.; Leech, D. *Phys. Chem. Chem. Phys.* **2012**, *14*, 14667–14672.
(30) Pan, L. J.; Yu, G. H.; Zhai, D. Y.; Lee, H. R.; Zhao, W. T.; Liu, N.; Wang, H. L.; Tee, B. C. K.; Shi, Y.; Cui, Y.; Bao, Z. N. *Proc. Natl. Acad. Sci. U.S.A.* **2012**, *109*, 9287–9292.
(31) Zhai, D. Y.; Liu, B. R.; Shi, Y.; Pan, L. J.; Wang, Y. Q.; Li, W. B.; Zhang, R.; Yu, G. H. *ACS Nano* **2013**, *7*, 3540–3546.
(32) Merchant, S. A.; Tran, T. O.; Meredith, M. T.; Cline, T. C.; Glatzhofer, D. T.; Schmidtke, D. W. *Langmuir* **2009**, *25*, 7736–7742.
(33) Nien, P.-C.; Wang, J.-Y.; Chen, P.-Y.; Chen, L.-C.; Ho, K.-C. *Bioresour. Technol.* **2010**, *101*, 5480–5486.
(34) Wang, J. In *Analytical Electrochemistry*, third ed.; Wiley–VCH: New York, 2006; p 39.
(35) Mao, F.; Mano, N.; Heller, A. *J. Am. Chem. Soc.* **2003**, *125*, 4951–4957.
(36) Sek, S.; Tolak, A.; Misicka, A.; Palys, B.; Bilewicz, R. *J. Phys. Chem. B* **2005**, *109*, 18433–18438.
(37) Yaghoubian, H.; Karimi-Maleh, H.; Khalilzadeh, M. A.; Karimi, F. *Int. J. Electrochem. Sci.* **2009**, *4*, 993–1003.
(38) Bard, A. J. In *Electrochemical Methods: Fundamentals and Applications*, 2nd ed.; John Wiley & Sons: New York, 2000; p 103.
(39) Bard, A. J. In *Electrochemical Methods: Fundamentals and Applications*, 2nd ed.; John Wiley & Sons: New York, 2000; p 115.
(40) Malitesta, C.; Palmisano, F.; Torsi, L.; Zambonin, P. G. *Anal. Chem.* **1990**, *62*, 2735–2740.
(41) Wang, H.; Wang, X.; Zhang, X.; Qin, X.; Zhao, Z.; Miao, Z.; Huang, N.; Chen, Q. *Biosens. Bioelectron.* **2009**, *25*, 142–146.
(42) Rogers, M. J.; Brandt, K. G. *Biochemistry* **1971**, *10*, 4624–4630.
(43) Senel, M. *Synth. Met.* **2011**, *161*, 1861–1868.
(44) Le Goff, A.; Moggia, F.; Debou, N.; Jegou, P.; Artero, V.; Fontecave, M.; Jousselme, B.; Palacin, S. *J. Electroanal. Chem.* **2010**, *641*, 57–63.

(45) Nagarale, R. K.; Lee, J. M.; Shin, W. *Electrochim. Acta* **2009**, *54*, 6508−6514.
(46) Chen, M.; Diao, G. *Talanta* **2009**, *80*, 815−820.
(47) Qiu, J.-D.; Deng, M.-Q.; Liang, R.-P.; Xiong, M. *Sens. Actuators, B* **2008**, *135*, 181−187.
(48) Abasiyanik, M. F.; Senel, M. . *J. Electroanal. Chem.* **2010**, *639*, 21−26.
(49) Kandimalla, V. B.; Tripathi, V. S.; Ju, H. X. *Biomaterials* **2006**, *27*, 1167−1174.
(50) Wei, Z.; Li, Z.; Sun, X.; Fang, Y.; Liu, J. *Biosens. Bioelectron.* **2010**, *25*, 1434−1438.
(51) Zhou, H.; Yang, W.; Sun, C. *Talanta* **2008**, *77*, 366−371.
(52) Pham, X.-H.; Bui, M.-P. N.; Li, C. A.; Han, K. N.; Kim, J. H.; Won, H.; Seong, G. H. *Anal. Chim. Acta* **2010**, *671*, 36−40.
(53) Jin, L.; Zhao, Y. J.; Liu, X.; Wang, Y. L.; Ye, B. F.; Xie, Z. Y.; Gu, Z. Z. *Soft Matter* **2012**, *8*, 4911−4917.
(54) Nita, I. I.; Abu-Rabeah, K.; Tencaliec, A. M.; Cosnier, S.; Marks, R. S. *Synth. Met.* **2009**, *159*, 1117−1122.